Smart Materials and Structures

PAPER

A multifunctional hybrid extrinsic–intrinsic self-healing laminated composites

To cite this article: John Konlan *et al* 2023 *Smart Mater. Struct.* **32** 075006

View the article online for updates and enhancements.

You may also like

- Shape memory alloy reinforced vitrimer composite for healing wide-opened cracks
Hansan Suslu, Jizhou Fan, Samuel Ibekwe et al.
- Self-healing efficiency study of thermoset-thermoplastic polymer material
W H Choong, H H Hamidi and K B Yeo
- Repeatable self-healing of thermosetting fiber reinforced polymer composites with thermoplastic healant
Bodiuzzaman Jony, Mishal Thapa, Sameer B Mulani et al.

This content was downloaded from IP address 70.172.228.224 on 05/06/2023 at 14:07

IOP Publishing Smart Materials and Structures
Smart Mater. Struct. **32** (2023) 075006 (14pp) https://doi.org/10.1088/1361-665X/acd82c

A multifunctional hybrid extrinsic–intrinsic self-healing laminated composites

John Konlan[1], Xiaming Feng[1,2] and Guoqiang Li[1,*]

[1] Department of Mechanical & Industrial Engineering, Louisiana State University, Baton Rouge, LA 70803, United States of America
[2] College of Materials Science and Engineering, Chongqing University, 174 Shazhengjie, Shapingba, Chongqing 400044, People's Republic of China

E-mail: lguoqi1@lsu.edu

Received 13 February 2023, revised 11 May 2023
Accepted for publication 22 May 2023
Published 5 June 2023

Abstract

Damage healing in fiber reinforced thermoset polymer composites has been generally divided into intrinsic healing by the polymer itself and extrinsic healing by incorporation of external healing agent. In this study, we propose to use a hybrid extrinsic-intrinsic self-healing strategy to heal delamination in laminated composite induced by low velocity impact. Especially, we propose to use an intrinsic self-healing thermoset vitrimer as an external healing agent, to heal delamination in laminated thermoset polymer composites. To this purpose, we designed and synthesized a new vitrimer, machined it into powders, and strategically sprayed a layer of vitrimer powders at the interface between the laminas during manufacturing. Also, a thermoset shape memory polymer with fire-proof property was used as the matrix. As a result, incorporation of about 3% by volume of vitrimer powders made the laminate exhibit multifunctionalities such as repeated delamination healing, excellent shape memory effect, improved toughness and impact tolerance, and decent fire-proof properties. In particular, the novel vitrimer powder imparted the laminate with first cycle and second cycle delamination healing efficiencies of 98.06% and 85.93%, respectively. The laminate also exhibited high recovery stress of 65.6 MPa. This multifunctional composite laminate has a great potential in various engineering applications, for example, actuators, robotics, deployable structures, and smart fire-proof structures.

Supplementary material for this article is available online

Keywords: self-healing, vitrimer, shape memory polymer, laminated composite, low velocity impact, flame retardancy

(Some figures may appear in colour only in the online journal)

1. Introduction

Thermosetting polymers are well known for their unique high strength engineering products such as fiber reinforced composites and coatings due to their high crosslink density, high rigidity, high thermal stability, low creep, better wettability, chemical inertness, and high solvophobicity [1, 2]. Notwithstanding, thermosets are susceptible to crack initiation and propagation because of the brittleness of the thermosetting network. For example, for epoxy based laminated composites subjected to transverse low velocity impact, most of the time, the damage such as delamination is created easily, which cannot be visualized with the naked eye, making conventional

* Author to whom any correspondence should be addressed.

 © 2023 IOP Publishing Ltd

external repair a great challenge [3–5]. Thus, damage self-healing is highly desired for the sustainability of lightweight thermoset composite structures [6–8].

Damage self-healing in thermoset polymers can be widely categorized into extrinsic healing by adding external healing agent and intrinsic healing by polymer itself [9, 10]. So far, many extrinsic self-healing approaches have been used, including using liquid healing agent contained in various containers such as microcapsules, hollow fibers, and microvacuolar networks [11–16], or using solid healing agent such as thermoplastic particles and fibers [17–20]. The limitation for liquid healing agent is generally believed that it can only heal for one time and cannot heal wider-opened cracks [21, 22]. Although the high viscosity liquid healing agent may overcome the inability to heal widely open cracks [21], the limitation is that the space occupied by the liquid healing agent, once it flows into the crack space, leaves behind a void, which becomes a new defect. Although using the concept of close-then-heal (CTH), i.e. using shape memory effect (SME) to close the crack first, and then heal the closed crack extrinsically or intrinsically, which was first proposed by Li *et al* [23, 24], may heal wider opened cracks with a small amount of liquid healing agent, it still suffers from the problem that the crack cannot be healed multiple times. On the other hand, although thermoplastic healing agent can heal multiple times, the limitation with solid healing agent is that the addition of thermoplastic in a thermoset matrix makes the composite exhibit some properties that are unique to thermoplastic such as lower strength and stiffness, vulnerability to chemical attacks, among others. In order to maintain the advantage of thermoset, it is highly desired that the healing agent is also a chemically crosslinked thermoset network.

This is possible with the development of intrinsic self-healing thermoset polymers. One such a polymer is vitrimer based on covalent adaptable network. Since the terminology vitrimer was coined in 2011 by Montarnal *et al* [25], many vitrimers have been developed [26–37]. In recent years, a new development is multifunctional vitrimers which have high strength, high stiffness, shape memory, flame retardancy, and 3D printability [6, 38–41]. With the rapid development in vitrimers, we believe that chemically crosslinked vitrimers can be used as a thermoset healing agent in fiber reinforced thermoset composite laminates.

In addition to delamination healing, other functionalities in laminated composites such as shape memory, flame retardancy, and 3D printability are also highly desired. Because these properties are controlled by the polymer matrix, polymers with such capabilities are preferred to serve as the matrix. Recently, Feng and Li [42] synthesized a high temperature shape memory polymer (SMP) with excellent flame retardancy and 3D printability. In their work, a UV curable triacrylate monomer with thermally stable isocyanate ring was used to fabricate a highly crosslinked network. They used readily available commercial phosphine oxide to serve a dual functionality as both a photo-initiator and a flame-retardant structure. The UV curing of the SMP only took 40 s under 35% irradiation intensity (232 nm, ∼45 mW cm^{-2}). With additional post thermal curing at 280 °C for 3 h, the polymer has exhibited the glass transition temperature up to 277 °C, recovery stress up to 35.3 MPa, energy output up to 2.9 MJ m^{-3}, room temperature tensile strength up to 48.7 MPa, and room temperature compressive strength up to 370 MPa, in addition to excellent fire-proof property and 3D printability. It is noted that SMPs have found many potential applications. In addition to self-healing per the CTH strategy, SMPs have found many potential applications such as serving as proppant [43] and loss circulation materials [44] in oil & gas industry, as sealant in sealing joints and cracks in pavement and bridge deck [45], as suture or stent in medical industry [46–48], as solar panels and energy storage devices [49, 50], as deplorable structures [51], etc.

The purpose of this study is to develop a new multifunctional laminated composite with delamination healing, shape memory, impact tolerance, and flame retardancy. To this purpose, a new vitrimer is designed, synthesized, and characterized to serve as external healing agent, and the multifunctional polymer developed by Feng and Li [42] as the matrix in preparing laminated composite. It is well known that laminated composites are vulnerable to low velocity impact damage. Although various types of damages can occur such as matrix cracking, fiber/matrix interfacial debonding, delamination, and fiber fracture under a low velocity impact, delamination is common which can cause significant reduction in load carrying capacity. Therefore, healing delamination is highly desired. To achieve this objective, instead of mixing the vitrimer powders with the polymer matrix, which is usually the case in preparing healable laminated composites, we strategically spray the vitrimer powder at the interface between the laminas, so that a small amount of vitrimer healing agent can achieve considerable healing capabilities. The mechanical properties and functionalities of the prepared composite laminates are tested, and the results are analyzed.

2. Experimental

2.1. Materials

Tris[2-(acryloyloxy) ethyl] isocyanurate (TAI), photo-initiator Diphenyl(2,4,6-trimethylbenzoyl) phosphine oxide (97%) (TPO), 2-hydroxy-2-methylpropiophenone (97%) (HMP), Bisphenol A glycerolate dimethacrylate (BAGDM), Bisphenol A glycerolate (1 glycerol/phenol)-diacrylate (BAGD), and 5-Amino-1,3,3-trimethylcyclohehane methylamine (AT) were purchased from Sigma-Aldrich to synthesize the vitrimer healing agent and the multifunctional polymer matrix. Unidirectional Saertex glass fiber (USGF) was purchased from Fiberglast USA and used as received as reinforcement.

2.2. Fabrication of thermoset composite laminate

To prepare the vitrimer healing agent, 100 g of Bisphenol A glycerolate (1 glycerol/phenol) diacrylate (BAGD) and 17.6 g of 5-Amino-1,3,3-trimethylcyclohexanemethylamine (AT) was rapidly mixed together and cured in an oven at 90 °C for 24 h (figure S1(a)). The cured sample, as shown in figure

S1(c) was then ball milled in a ball milling machine (PQ-N2 Planetary Ball Mill, Across International) for 48 h to produce vitrimer powder with mesh size of 100–250 nm as shown in figure S1(j). The vitrimer powder was bagged and later used as healing agent.

Unidirectional Saertex glass fiber was cut into eight (8) square shape with dimensions 216 mm × 216 mm, as illustrated in figure S1(b).

To prepare the polymer matrix for the laminated composite, we followed Feng and Li [42]. In brief, 93 wt % tris[2-(acryloyloxy) ethyl] isocyanurate (TAI) monomer and 7 wt% photo-initiator diphenyl(2,4,6-trimethylbenzoyl) phosphine oxide (TPO) was mixed at 100 °C for 2 h at 120 rpm-shown in figure S1(d), mixing at this rate prevents the formation of bubbles. The homogeneously mixed TAI monomer and TPO photo initiator was then used to wet through the unidirectional Saertex glass fibric, and to achieve 50% fiber volume fraction, as shown in figure S1(e). After that, 0.5 g vitrimer powders were sprayed uniformly on the top surface of each polymer wetted glass fabric layer, as illustrated in figure S1(f). Eight layers of the prepared individual plys were then rolled together. A total of 4 g of the vitrimer powder was used as healing agent in preparing the eight-layer composite laminate. The weight fraction of the vitrimer powder was 3%. The vitrimer powder doped laminate was then moved with the aid of an aluminum (Al) foil to an open aluminum frame of 216 mm × 216 mm × 5.08 mm. The aluminum foil was gently removed from the frame as seen in figure S1(f). The open frame was then covered with tempered plain glass sheets on the top and bottom. Two open plastic frames having the same dimension as the aluminum frame were placed on the top and bottom of the plain glass sheets. Four C-clamps were used to apply appropriate pressure to hold the laminate in the transparent glass slabs as shown in figure S1(g). The clamped laminate was then cured in a UV chamber (intel-liRay 600, Uvitron international, USA) for 40 s under 35% irradiation intensity (232 nm, ∼45 mW cm^{-2}) [52], figure S1(h). The cured laminate was then cut into 5 rectangular specimens of dimension 152.40 mm × 25.40 mm × 5.08 mm using a water jet machine, as shown in figure S1(i). All the above processes were repeated to fabricate more samples for characterization, mechanical and functional testing, self-healing and flame retardancy testing. Also, similar approach was adapted to prepare the control samples, but this time round, without the addition of vitrimer powders. In the following, the laminate consisting of the vitrimer healing agent is named as GFRP-TAITPOVP (glass fiber reinforced polymer (GFRP) - TAI-TPO-Vitrimer Powder (VP)), while the laminated composite without the vitrimer healing agent is named as GFRP-TAITPO.

2.3. Compositional analysis, thermal analysis, and thermomechanical analysis

PerkinElmer 4000 differential scanning calorimeter (DSC) (MA, USA) was used to study the thermal behavior of the vitrimer. Samples with weight (5–10 mg) were heated and cooled at a linear heating/cooling rate of 10 °C min^{-1} in the sample holder; the isothermal time at the end of heating or cooling was 3 min. The purge rate of the nitrogen gas used was 30 ml min^{-1}. TGA 550 Discovery Series Thermal Analyzer (TA Co., USA) was used to conduct non-isothermal thermogravimetric analysis (TGA) tests. The temperature ramped from 20 °C to 800 °C at a heating rate of 10 °C min^{-1} in air environment. The purging rate of the gas was 40 ml min^{-1}. Nicolet 6700 FTIR spectrometer (Thermo Fisher Scientific, USA) was used to conduct Fourier transform infrared spectroscopy (FTIR) analysis and the spectra were collected in attenuated total reflection mode by collecting 32 scans from 400 to 4000 cm^{-1}. Scienta Omicron ESCA 2SR x-ray Photoelectron Spectroscope was used to obtain the x-ray photoelectron spectroscopy (XPS) spectra.

2.4. Low velocity impact and compression after impact (CAI) test

Low velocity impact tests were conducted by using Instron Dynatup 8250 HV impact tester per ASTM standard D3763-18. The dimension of the specimens was 152.40 mm × 25.40 mm × 5.08 mm. With a hammer weight of 11.2 kg and a drop height of 205 mm, the impact velocity was 2 m s^{-1} and impact energy was 22.4 J. The impact was at the center of the specimen. The sensors integrated in the impact tester were used to obtain the impact force, deflection, and velocity change with time, and from which the absorbed energy can be calculated. After low velocity impact tests, CAI tests were conducted by uniaxial compression till buckling of the impact damaged specimens using a QTEST 150 machine. The CAI tests were conducted using a strain-controlled mode at a loading rate of 1.3 mm min^{-1}, at room temperature. The buckling load was used to evaluate the damage and healing efficiency. A minimum of five specimens with a dimension of 152.40 mm × 25.40 mm × 5.08 mm were tested by low velocity impact and CAI.

2.5. Shape memory effect (SME) test

In order to investigate the SME of the novel laminated composite, hot programming by three-point bending test was performed (figure S2) by using an eXpert 2610 MTS (ADMET, Norwood, MA, USA) equipped with a temperature regulated oven. During programming, the specimen and the three-point bending fixture were inserted into the oven at room temperature. The temperature was then heated to 250 °C, and held for 30 min. Three-point bending was then conducted at a loading rate of 2 mm min^{-1}. The deformed beam was held at 250 °C for 20 min. The temperature was then lowered to room temperature while holding the deflection constant. To complete the hot programming process, unloading was conducted at room temperature. To avoid thermal expansion of the metal fixtures during stress recovery test, the MTS fixtures were pre-heated to 250 °C. Then the programmed bent specimen was rapidly inserted in between the fixtures. The recovery force change with time were recorded by the load cell. The shape fixity ratio (F_r) and shape recovery ratio (R_r) were determined by using equations (1) and (2), respectively. The recovery stress was determined by using the bending stress formula from beam theory as given in equation (3)

$$F_r = \frac{\varepsilon_f}{\varepsilon_l} \times 100\% \quad (1)$$

$$R_r = \frac{\varepsilon_f - \varepsilon_r}{\varepsilon_f} \times 100\,\% \quad (2)$$

$$\sigma_{\max} = \frac{3}{2}\frac{PL}{bh^2} \quad (3)$$

where ε_l is the maximum bending strain during hot programming, ε_f is the strain that has been fixed after the load is removed, and ε_r is the residual strain after free shape recovery. And $\sigma_{\max,}$ is the bending stress, P is the maximum bending load, L is the span length, b is the width and h the thickness of the composite laminate beam.

2.6. Recycling and healing efficiency

The class of vitrimers such as bisphenol A glycerolate dimethacrylate has a notable recycling efficiency [31, 52, 53]. In this work a novel vitrimer was synthesized and converted to powders by ball milling and used as healing agent at the interfaces between the laminas. The healing efficiency of the impact damaged and healed laminates is defined as the ratio of the maximum impact force (MIF) of the healed laminate to the ratio of the pristine specimen; and the ratio of the critical buckling loads (CBL) of the healed specimen to that of the pristine sample are also used to evaluate the healing efficiency, which are given as:

$$[\text{Healing efficiency}]_{\text{IL}} = \frac{E_{\text{LR}}}{E_{\text{LO}}} \times 100\% \quad (4)$$

$$[\text{Healing efficiency}]_{\text{CAI}} = \frac{P_{\text{LR}}}{P_{\text{LO}}} \times 100\% \quad (5)$$

where E_{LR} is the peak load of the recycled composite laminate and E_{LO} is the peak load of the pristine composite laminate before damage And P_{LR} is critical buckling load of the healed composite laminate and P_{LO} is the critical buckling load of the pristine composite laminate before healing.

During healing test, the healing temperature used was 170 °C, the healing pressure was 20 MPa, the healing time was 1 h. The impact damaged composite laminates were sandwiched between two rectangular tool-grade stainless-steel plates with the same dimension as the laminate that were in the soaked oven at 170 °C. This was done to achieve a higher degree of transesterification of the vitrimer in mending the interfacial delamination. It is interesting to note that, dynamic covalent exchange occurs in this vitrimer via both dynamic (retro) aza-Michael reaction and catalyst free transesterification [54].

2.7. Scanning electron microscopy (SEM) examination

The degree of delamination, fiber breakage and matrix cracking of the composite laminates were evaluated using JSL-6610 LV, JEOL USA. The surface of the damaged and healed samples was sputtered with gold, approximately 5 nm thick in order to avoid charging during the analysis. Accelerating voltage of 20 kV and a working distance of 8 mm—10 mm with a magnification of 500× were used.

2.8. Flame retardancy test

A simple vertical burning experiment was used to evaluate the flame retardancy of the composite laminate. The dimension of the rectangular specimen was 125 mm × 13.5 mm × 3.2 mm, which was determined based on the UL-94 standard for safety of flammability of plastic materials used in devices. The control specimen, which was made from bisphenol A glycerolate dimethacrylate (BPAGMA) reinforced with Saertex unidirectional glass fiber, was also tested similarly by a gas burner for 10 s. A camera was used to record the whole combustion processes.

3. Results and discussions

3.1. FTIR

FTIR spectra of the composite laminate was determined. Also, that of the TAI and TPO monomer mixture was also investigated; see figure 1.

From figure 1, the blue line gives the spectrum of the TAI and TPO monomer mixture, whereas the black line is the spectrum of the fully cured composite. The FTIR results show that, the monomer mixture contained –C=C– double bonds at wavenumbers 1450 cm^{-1}–1600 cm^{-1} and also at 900 cm^{-1}–800 cm^{-1} [42]. The degree of curing of the matrix determines the strength of a composite laminate because it bonds the fiber reinforcements together. From figure 1, it is seen that most of the double bonds are broken rigorously. This signifies good conversion or crosslinking of the double bonds as can be seen from significant reduction of the double bonds in the spectrum of the composite. As discussed by Feng and Li [42], complete conversion of the matrix needs further post-thermal curing at 280 °C for 3 h.

3.2. Thermal properties

It has been well established that, polymers with high glass transition (T_g) temperature value tend to have higher dimension stability and maintain mechanical performance at elevated temperatures. DSC studies with two heating and cooling cycles were conducted on the VP polymer and the glass fiber reinforced composite laminate (GFRP-TAITPOVP) between −30 °C to 300 °C (figure 2). In figure 2, both the first heating cycle and second heating cycle are shown for the composite laminate. For the composite, the first heating cycle shows a clear exothermic peak (∼285 °C) attributed to thermal polymerization of C=C groups. This suggests that further crosslinking occurs in the polymer matrix, which is in agreement with Feng and Li [42], who used 280 °C to post-cure the polymer after UV curing. Also, the glass transition temperature of the UV cured composite is about 219.7 °C. As demonstrated by Feng and Li [42], by UV curing alone, which is also the case in the current study, the glass transition temperature of the polymer matrix is broad, and the highest is about 220 °C.

From the second cycle, it is seen that the glass transition temperature (T_g) of the GFRP-TAITPOVP composite was determined by extrapolation using the first derivative and

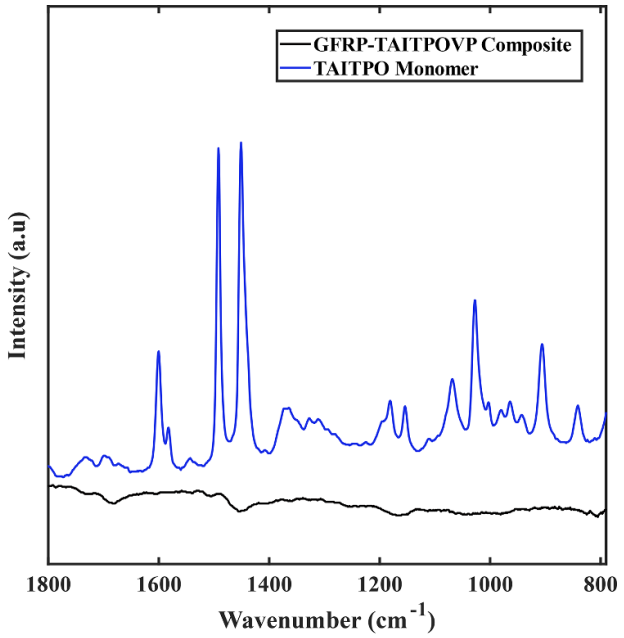

Figure 1. FTIR spectrum of the TAI and TPO monomer (TAITPO) and the composite laminate, signifying curing of the composite laminate.

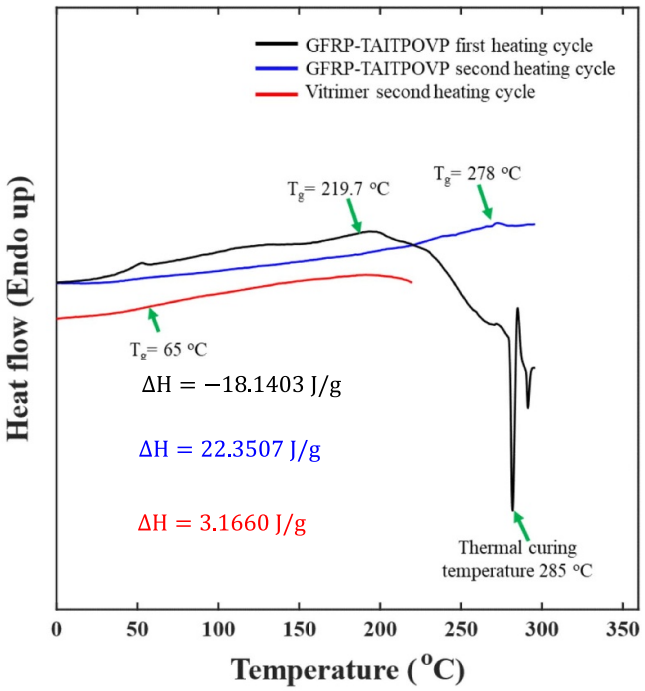

Figure 2. The first and second heating cycle for the heat flow profile of the GFRP-TAITPOVP composite and the second heating cycle for the heat flow profile of the vitrimer healing agent characterized by DSC, with the enthalpy of reaction (ΔH) as -18.1403 J g^{-1}, 22.3507 J g^{-1}, and 3.1660 J g^{-1}, for the first heating cycle of the GFRP-TAITPOVP composite, the second heating cycle of the GFRP-TAITPOVP composite, and the second heating cycle of the vitrimer healing agent, respectively.

was found to be 278 °C. This again shows that, after the first heating cycle, the polymer matrix was post cured, which increased the glass transition temperature to about 280 °C, and again agrees with the test results by Feng and Li [42]. For the vitrimer, with a T_g of 65 °C, it provides an excellent window for healing. Thus, a healing temperature of 170 °C was selected for healing the UV cured GFRP-TAITPOVP composite laminate. At this healing temperature, the composite is still in glassy state and is still stable and stiff because the healing temperature is still well below the T_g of the composite (about 219.7 °C). Usually for most intrinsic healing, the mechanical properties of the specimen are compromised because the polymer is in a rubbery state.

To demonstrate the thermal stability of the GFRP-TAITPOVP composite laminate, the thermal stability of the pure TAITPO polymer and that of the vitrimer was also studied under inert nitrogen atmosphere in non-isothermal mode, as shown in figure 3. Figure 3(a) shows the non-isothermal thermogravimetric (TG) and figure 3(b) gives the corresponding derivative of TG (DTG) curves. From room temperature to about 250 °C, weight loss for both the pure TAITPO polymer and the composite GFRP-TAITPOVP is negligible. As for the VP, from room temperature to about 180 °C, the weight loss was also negligible. This finding is interesting and of great significance, since it further validates the choice of the healing temperature for the GFRP-TAITPOVP composite laminate at 170 °C.

Most reported healing agents in the literature compromise the mechanical properties such as the stiffness when heated to form a melt. In our case, the thermal stability of the polymer matrix hosting the reinforcement is guaranteed, making the healing of the laminate possible without compromising the mechanical integrity of the laminate.

The initial decomposition temperature ($T_{2\%}$) corresponding to 2% weight loss of the TAITPO polymer was extrapolated to be around 405.30 °C, whereas that of the composite and vitrimer powder was found to be 348.20 °C and 267.80 °C, respectively. The weight loss is usually initiated by the decomposition and degradation of the weak and unstable bonding, hydroxyl group, the unreacted epoxy, and any other impurities that might be present. When present, they will begin to degrade at their decomposition temperature. A remarkable weight loss is recorded at temperatures above 456 °C, which is also the highest peak temperature (T_{max}) in the derivative TG curve in figure 3(b). Most SMPs have their T_{max} around 300 °C–420 °C [55], thus with the TAITPO SMP, a huge improvement in thermal stability can be achieved.

3.3. Shape memory effect (SME)

The shape memory behavior of the composite laminate was determined using three-point bending test, since the laminate had a good deformability in this mechanical response mode. The programming was carried out using a laminate with a dimension of 114 mm × 12.5 mm × 5.08 mm. Figure S3 show the images of the composite laminate prior to bending programming, during bending programming, after bending programming, and after free shape recovery, respectively. The shape fixity ratio was calculated to be 67.3%. And the shape

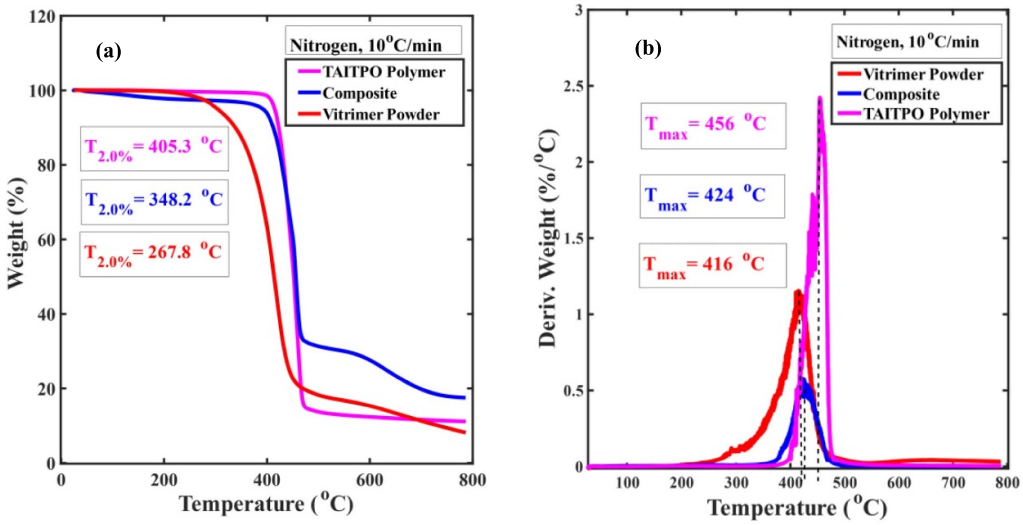

Figure 3. (a) TG curves of TAITPO polymer, GFRP-TAITPOVP composite, and vitrimer powder, and (b) DTG curves of TAITPO polymer, GFRP-TAITPOVP composite, and vitrimer powder.

recovery ratio was found to be 98.5% through free recovery test at 250 °C. This suggests that the composite laminate can almost recover to its original shape under free shape recovery. The entire thermomechanical cycle (programming and constrained stress recovery) is shown in figure 4. For convenience, the hot programming load vs displacement profile of the composite specimen is shown in figure 5(a). The maximum programmable bending stress was estimated using equation (3) in section 2.4. Given a specimen with a dimension of 114 mm × 12.5 mm × 5.08 mm, and maximum programming load of 509 N as presented in figure 5(a), for a three-point bending programming with a span length of 67.5 mm, the maximum bending stress for the hot programming is calculated as 157.56 MPa. For the maximum bending stress in terms of fully constrained stress recovery, the maximum bending load in figure 5(b) was used with the other parameters kept the same. The maximum recovery bending stress was computed as 65.60 MPa.

To put the SME of this composite in a broader view, we reviewed several typical SMPs and SMP composites, and compared their recovery stresses. The results are shown in figure 6. From figure 6, it is seen that the recovery stresses cover a broad range, based on if they are pure polymers or polymer composites. It is also seen that their glass transition temperatures also bridge a wide range. This provides a variety of choices for researchers and engineers to select pure SMPs or SMP composites based on their design needs.

It is noted that the pure polymer matrix in this study has good SME, with a shape fixity ratio of 58.0% and shape recovery ratio of 93.1% [42]. As compared to the laminated composite, which has a shape fixity ratio of 67.3% and shape recovery ratio of 98.5%, it is seen that the incorporation of glass fibers slightly improved the SME of the SMP matrix. Although the vitrimer healing agent is also incorporated in the composite, it is believed that its effect on the SME of the composites is negligible due to its very small amount (3% by weight) used.

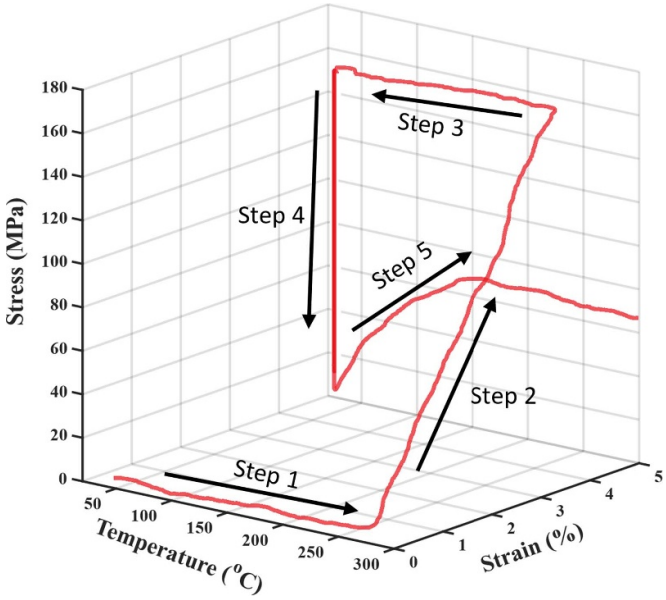

Figure 4. Five-step thermomechanical cycles for the GFRP-TAITPOVP Composite. Step 1: heating. Step 2: high temperature loading. Step 3: cooling. Step 4: unloading. Step 5: fully constrained stress recovery.

3.4. Flame retardancy

According to the thermogravimetric analysis in section 3.2, it is evident that the GFRP-TAITPOVP composite laminates have excellent thermal stability. The incorporation of the excess amount of 7 wt% TPO (photo-initiator) enhanced the TAI polymer matrix with exceptional flame retardancy. The flame-retardancy property of the GFRP-TAITPO composite laminate can eliminate, if not completely, can reduce the use of protective layers in mass and heat transfer process, which is a key requirement for aerospace and other lightweight structural applications. Most SMPs and composites do not have this intrinsic flame retardancy [62]. For example, fiber rein-

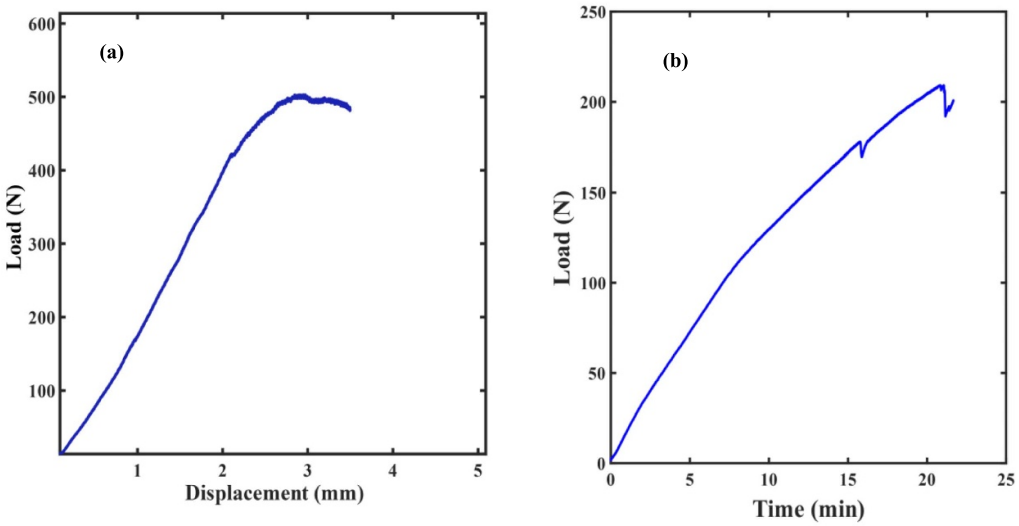

Figure 5. (a) Hot programming profile of the composite laminate under three-point bending, (b) The fully constrained stress recovery profile of the composite laminate.

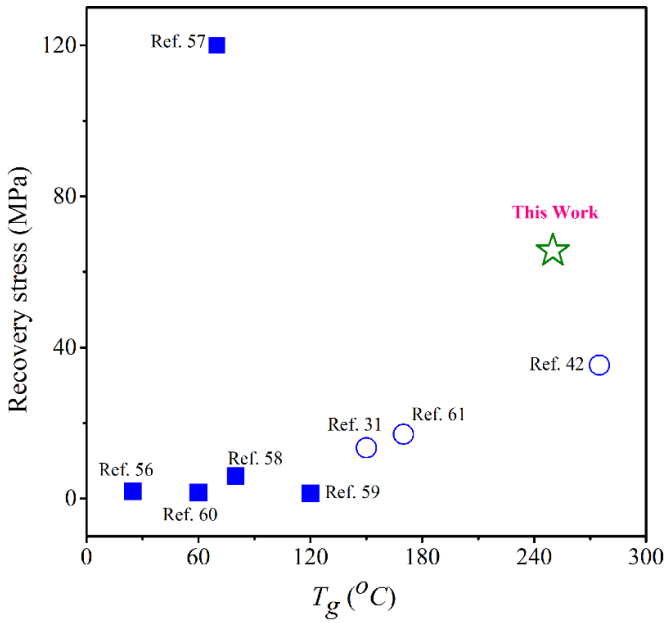

Figure 6. Comparison of the recovery stress and T_g value of our SMP based composite with SMPs or SMP based composites reported in the literature (the blue circle means pure SMPs and the blue square means SMP (nano)composites) [31, 42, 56–61].

forced bisphenol A glycerolate dimethacrylate (BPAGMA) SMP composite laminates are highly flammable. To demonstrate this, unidirectional Saertex glass was used as reinforcement in the BPAGMA polymer matrix to fabricate GFRP-BPAGMA composite laminate as control specimens for flame retardancy test. Figures 7(a) and (b) illustrate the combustion process of the GFRP-TAITPOVP composite laminate and the control. The ignition lasted for 10 s. During this ignition time period, the GFRP-TAITPOVP specimen tries to resist combustion, whereas the control begins to burn rapidly. At 10 s of ignition, the GFRP-TAITPOVP specimen is still not ignited. On the contrary, the GFRP-BPAGMA control specimen is covered with flames. When the burner is removed at 10 s, the GFRP-TAITPOVP specimen extinguishes by itself, while the GFRP-BPAGMA control specimen burns continuously.

To further investigate the flame-retardant mechanism, XPS characterizations for the char residue from both the smart composite and the control composite was analyzed. The results for the XPS spectra of the char residue for both the GFRP-TAITPOVP and that of the control are reported in figure S4. The spectra of the char residue from each type of laminates mainly contain C, N, O, and P. The high-resolution XPS spectra of these elements illustrate the surface chemistry and the binding properties. From figure S4(a), it can be seen that, the relative intensity (a.u) of C 1 s in the GFRP-TAITPOVP composite at binding energy 286.6 eV is much higher than that of the GFRP-BPAGMA control. The same observation is made for N, O, and P at their respective binding energies from figures S4(b)–(e), respectively.

These observations validate the snapshots from figure 7, with emphasis on the photo taken at 11 s. It can be seen clearly that the highly flammable control specimen was burnt severely. Based on the thermal stability test results and the molecular structures evolution during combustion, it is believed that the thermally stable isocyanurate and phosphine oxide structures contribute to the formation of rigid protective char layer. The char layer can delay the thermal decomposition and prevent the heat transfer from combustion area to the substrate, and also slow down the escape of combustible pyrolysis volatiles, which help reduce the fire hazard of the GFRP-TAITPOVP composite laminate. Hence, it can be deduced that GFRP-TAITPOVP composite is flame retardant.

3.5. Impact test and CAI test results

The load and energy required to break a specimen are commonly used to evaluate the impact properties. The typical load and energy traces for the GFRP-TAITPOVP and that of the control laminates (GFRP-TAITPO) subjected to low velocity

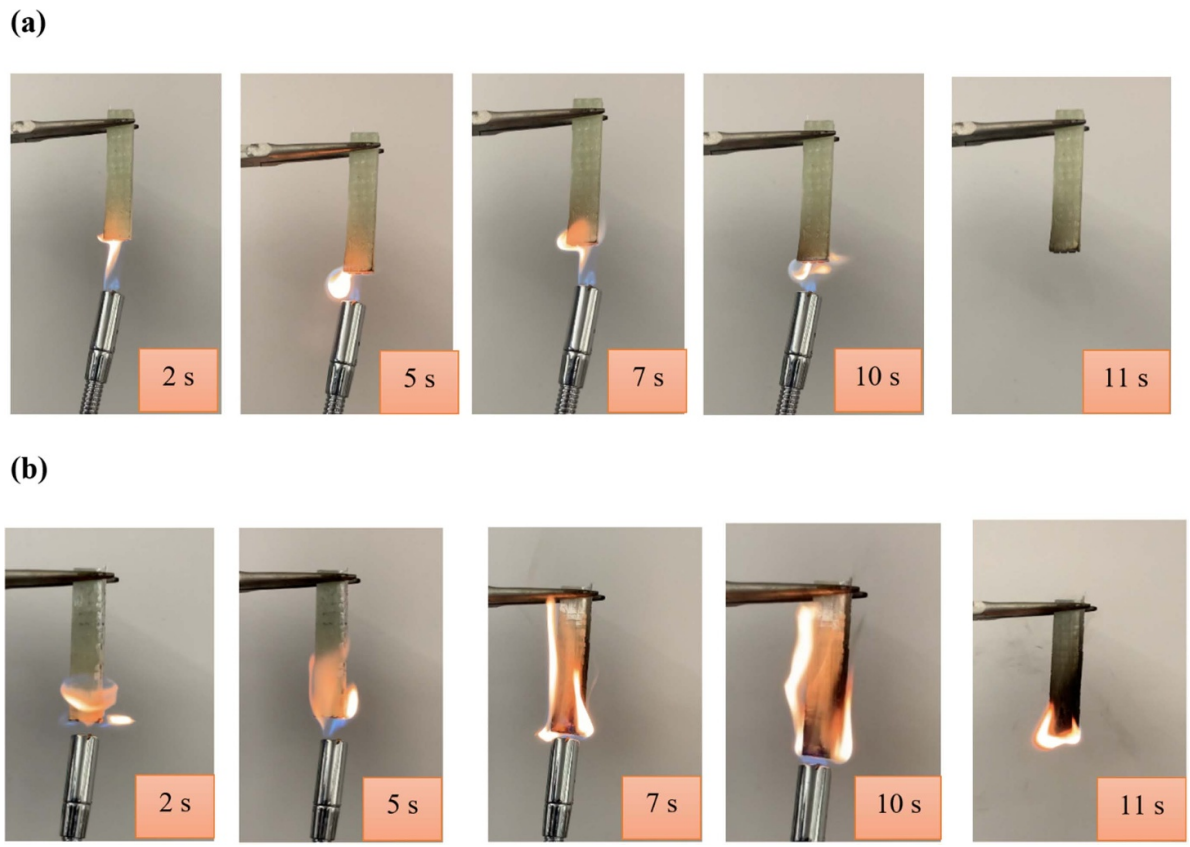

Figure 7. Combustion behavior of (a) GFRP-TAITPOVP composite laminate, and (b) GFRP-BPAGMA control composite laminate.

impact are discussed in this section. To evaluate the impact tolerance of the laminates, the maximum impact force, crack initiation energy (CIE) and crack propagation energy (CPE) are the most significant parameters. Illustrated in figure 8 are the typical force–time and energy–time histories of the fabricated GFRP-TAITPOVP and GFRP-TAITPO laminates under low velocity impact test. Presented in table 1 is the summary of the CIE and CPE recorded from the low velocity impact tests. According to the literature [53] and ASTM Standard D3763-18, the ability for a target to transmit energy elastically is measured by the CIE, and the energy absorbed by the target during damage creation and propagation is evaluated by the CPE. The initiation energy is defined as the impact energy corresponding to the maximum impact force. And the propagation is calculated by taking the difference between the maximum impact energy and the initiation energy. Thus, it can be deduced that, a large value of CIE and a small propagation energy suggest a high impact tolerance [63, 64].

From figure 8 and table 1, it can be observed that the GFRP-TAITPOVP composite laminates have improved impact load and CIE of about 25.4% and 52.80%, respectively, as compared to those of the GFRP-TAITPO control laminate. From literature, improved interlaminar strength is achieved by incorporation of micro/nano particles [64]. The particulate reinforcement of the GFRP-TAITPOVP laminate with the vitrimer powders resulted in an improved CIE. It is interesting to note that the approach in this work is novel since most of the micro/near nano particulate reinforcements utilize inorganic rigid particles such as carbon nanotubes, or graphene, silica and clay particles [64–66]. This new discovery can provide a niche for recycling existing vitrimers into powders and using them as particulate reinforcements in many engineering applications. The vitrimer powders reduced the brittleness of the TAITPO epoxy matrix and introduced some ductility which consequently improved the CIE of the GFRP-TAITPOVP laminate. From the literature of impact on composite materials [63, 64, 67], the more brittle the laminate, the lower the CIE, and the more ductile the laminate, the higher the initiation energy. The appreciable reduction in propagation energy implies that the Vitrimer powder not only serve as healing agent but also micro particulate reinforcement. The particles form pinning points and thus, constrain the crack propagation, leading to a reduction in delamination opening. These observations can be validated by SEM images in figure 9(a), SEM image of GFRP-TAITPOVP composite laminate after impact, and figure 9(b), SEM image of GFRP-TAITPO control laminate after impact. It is clear that the control laminate has larger and wider delamination, suggesting severe damage.

On the other hand, the laminate reinforced with the vitrimer micro particles experienced less damage with much smaller and narrower delamination. This observation falls in line with the CPE from the impact test. It is interesting to note that, the vitrimer powders not only serve as healing agent but

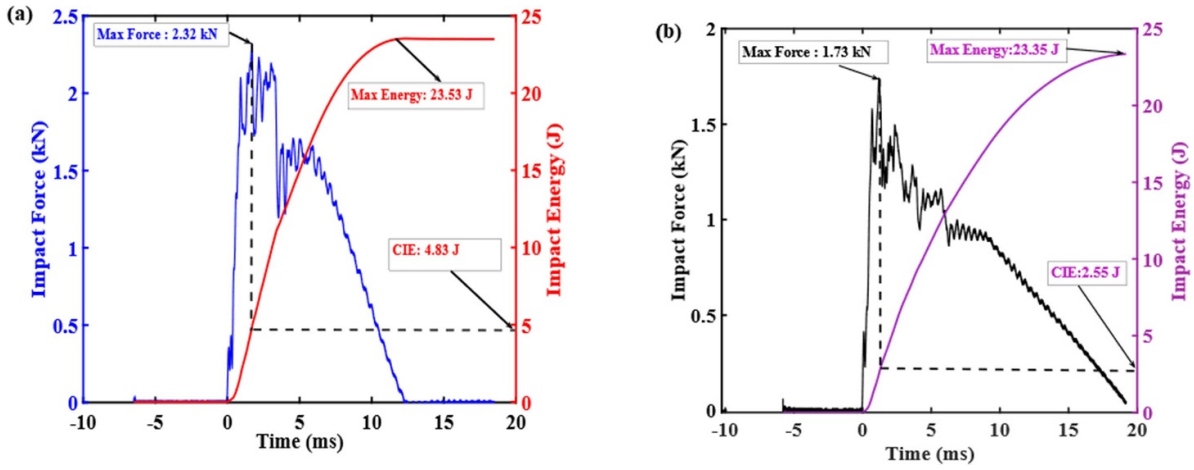

Figure 8. Typical force and energy histories during low velocity impact test on (a) GFRP-TAITPOVP composite laminate, and (b) GFRP-TAITPO control composite laminate.

Table 1. Impact test results of laminates subjected to an impact energy of 23.5 J.

Composite type	Impact location	Initiation energy (J)		Propagation energy (J)		Max impact force (kN)	
		Average	Sd	Average	Sd	Average	Sd
GFRP-TAITPOVP	Center	4.83	1.24	18.70	1.19	2.32	0.18
GFRP-TAITPO	Center	2.55	1.35	20.80	1.26	1.73	0.15

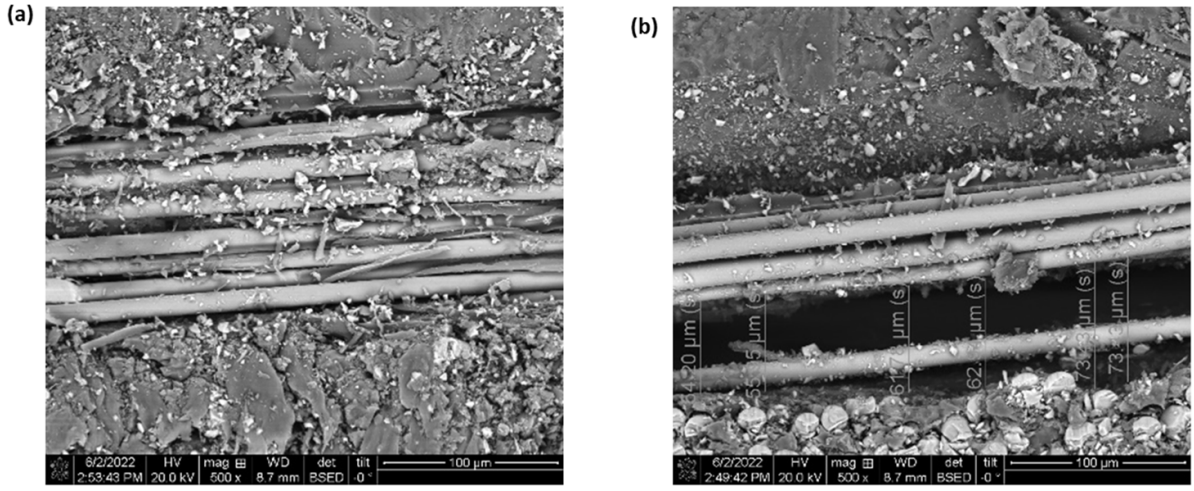

Figure 9. Scanning electron microscopy of (a) GFRP-TAITPOVP composite laminate after impact, with minor delamination, and (b) GFRP-TAITPO-control laminate after impact, with severe delamination.

also particulate reinforcement to mitigate crack propagation and delamination opening.

The CAI test of the GFRP-TAITPOVP and the GFRP-TAITPO composite laminates was conducted after impact tests. The buckling load in the CAI test was used as the measurement to determine the load carrying capacity of each group of the impacted laminates. Figure 10 illustrates typical load–displacement response of the CAI test results of the composites laminates. From figure 10, it can be observed that, the buckling load for the GFRP-TAITPOVP composite laminate is 1.5 times that of the GFRP-TAITPO control laminate. In other words, the GFRP-TAITPOVP laminate has about 33% more load carrying capacity before buckling. The substantial increase in buckling resistance is due to the small delamination in the GFRP-TAITPOVP composite laminate. From the literature, it is well known that delamination reduces the flexure stiffness of the laminate, leading to buckling at lower axial loads. This test also validates that vitrimer powders help in resisting delamination propagation, and thus increasing the CAI strength of the GFRP-TAITPOVP composite laminate.

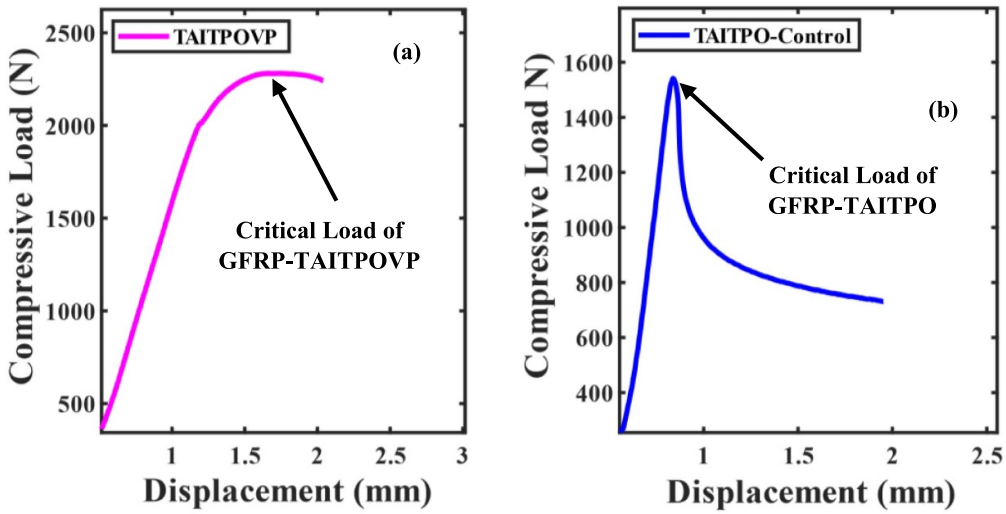

Figure 10. Typical compression load versus displacement during compression after impact (CAI) test (a) GFRP-TAITPOVP composite laminate and (b) GFRP-TAITPO-Control laminate.

3.6. Healing efficiency

The healing/recycling efficiencies of vitrimer based SMPs is well documented in the literature [31]. Investigating the recycling/healing efficiency of vitrimers involves direct estimation of the load carrying capacity of the pristine and recycled vitrimer. The maximum impact loads sustained in the low velocity impact test and CAI test of the pristine and recycled laminate were previously used to calculate the healing/recycling efficiency. The method of healing adopted in this work is that, the delamination in the impacted laminates were first closed and then healed by following the 'Close Then Heal' (CTH) strategy [23, 24]. The CTH approach is used since it is suitable for healing wider opened cracks, such as delamination in laminated composites. The CTH strategy is a biomimetic two-step mechanism, which involves closing or narrowing the crack first, followed by healing extrinsically or intrinsically. In this study, external pressure was used to help close the delamination. A pressure of 20 MPa was used to bring the delaminated laminate in touch, and the laminate is healed by hybrid extrinsic/intrinsic healing, meaning vitrimer as an external healing agent, which is extrinsic healing, and the healing of the vitrimer itself is based on transesterification reaction, which is intrinsic.

After the first healing, the specimens were tested by the same low velocity impact and CAI tests again for the second healing cycle. Figures S5(a) and (b) show the impact responses of the GFRP-TAITPOVP composite laminate after the first and second healing cycles, respectively. Figures S6(a) and (b) show the impact responses of the GFRP-TAITPO control composite laminate after the first and second healing cycles, respectively. Figures S7(a) and (b) show the load-displacement curves of the two types of laminates under CAI test, respectively.

From figures S5, S6, and table 2, it is seen that, the first cycle healing efficiency in terms of the maximum impact force (MIF) is about 81% for the GFRP-TAITPOVP and that for the control laminate is just only about 60%. For the second healing cycle, the efficiency of the GFRP-TAITPOVP dropped to about 68%, whereas that of the control specimen reduced to 56%. Thus, the vitrimer powders improves the healing efficiency of the GFRP-TAITPOVP laminate significantly.

Also, from figure S7 and table 2, it can be observed that the first cycle healing efficiency in terms of the maximum critical buckling load (CBL) is about 98% and that of the control is just 75%. Again, the vitrimer powder healing agent restores the health of the laminate to almost that of the original level. After the second healing cycle, the vitrimer powder reinforced laminate still performed better than the first healing cycle of the control specimen.

The above deductions can be further validated by the SEM images presented in figures 11(a) and (b). From figure 11, it is clear that the delamination is closed and healed in the GFRP-TAITPOVP laminate, while the delamination in delaminated GFRP-TAITPO control laminate remains open and unhealed. Therefore, without the vitrimer healing agent, the partial recovery of the strength in the control composite GFRP-TAITPO was due to the narrowed delamination by the external pressure. No healing at all for the narrowed delamination because the polymer matrix does not have healing capability.

It is believed that the healing mechanism is due to the compatibilization reaction between the vitrimer powders and the epoxy matrix. Because the vitrimer has reversible covalent bonds, broken connections between neighboring vitrimer powders can be rebonded during healing. For the epoxy matrix, it does not have reversible covalent bonds, therefore, the vitrimer powders at the interlaminar interface cannot establish covalent bonds with the epoxy matrix. Instead, it is believed that the healing is due to diffusion of molecular segments of the vitrimer powders into the epoxy matrix, which establishes physical entanglement, similar to using thermoplastic particles as the healing agent [19].

Table 2. Summary of mechanical properties and healing efficiency after each healing cycle.

Composite type	Cycle	Crack initiation energy (CIE), J		Crack propagation energy (CPE), J		Max impact force (MIF), kN		Critical buckling load (CBL), N	Healing efficiency (%)	
		Average	SD	Average	SD	Average	SD	Average	MIF	CBL
GFRP-TAITPOVP	0	4.83	1.24	18.70	1.19	2.32	0.18	2281.90	100.00	100.00
	1	5.25	1.33	17.94	1.22	1.88	0.21	2237.52	81.03	98.06
	2	6.02	1.39	17.76	1.27	1.58	0.19	1960.78	68.10	85.93
GFRP-TAITPO-Control	0	2.25	1.35	20.80	1.26	1.73	0.15	1541.47	100.00	100.00
	1	5.12	1.46	14.68	2.75	1.03	0.17	1158.03	59.54	75.13
	2	5.25	1.52	16.34	2.32	0.97	0.13	1091.61	56.07	70.81

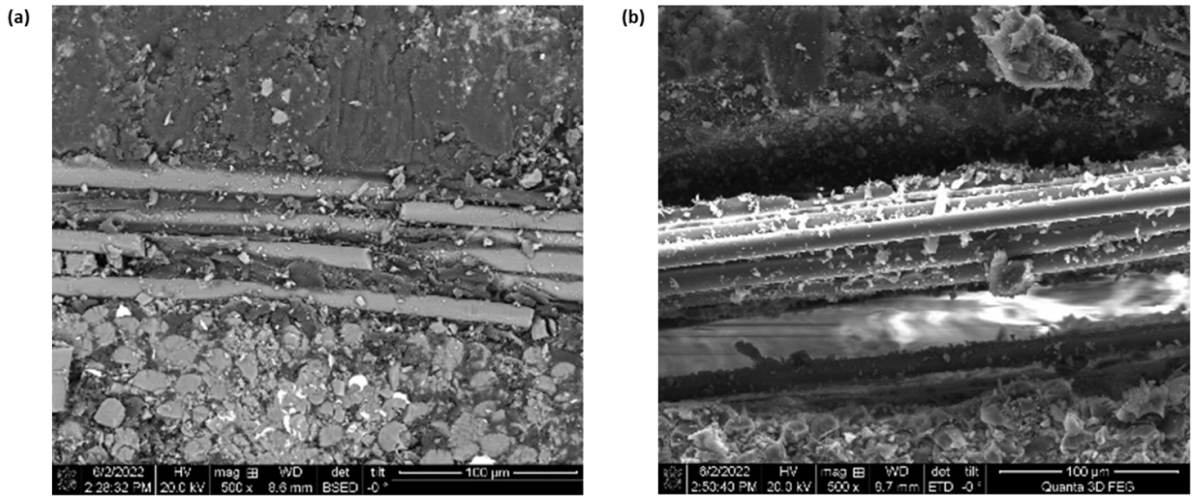

Figure 11. (a) Healed delamination in delaminated GFRP-TAITPOVP laminate, and (b) unhealed delamination in delaminated GFRP-TAITPO control laminate.

To further characterize the surface chemistry of the healed laminates of GFRP-TAITPOVP, XPS study was conducted. The high resolution XPS spectra of the elements present display the surface chemistry and the bonding characteristics. XPS spectra were recorded on the healed interface to explore the detailed condensed-phase mechanism (figures S8(a)–(d)). The C 1 s peaks centered at 289.1 eV, 287.3 eV and 284.6 eV are attributed to the C–O group, C=O group, C–C/C–H of the aliphatic and aromatic species, respectively. The O 1 s spectrum displays three peaks, the one at 532.1 eV is attributed to the P=O bond and the one at 534.2 eV is assigned to the C=O groups and 535.89 eV to C–O–C structure. The two peaks in P 2p spectrum at 133.7 eV and 132.8 eV is assigned to P=O structure in the healed GFRP-TAITPOVP laminate [68, 69].

Only one peak is shown in the N1s spectrum at 398.9 eV, which is attributed to the stable C–N bond in the isocyanurate with six-membered ring [70]. Based on the evolution of the molecular structures during healing, it is believed that the thermally stable isocyanurate and phosphine oxide structures contribute to the formation of intact bonds with the vitrimer powder healing agent. This leads to an effective and efficient healing of the GFRP-TAITPOVP composite laminate as reported in this section.

4. Conclusions

In summary, a novel multifunctional hybrid extrinsic/intrinsic self-healing composite laminate with delamination healing, shape memory, impact tolerance, and flame retardancy was designed, fabricated, and characterized successfully. The key is to use intrinsic self-healing vitrimer as the external healing agent. The vitrimer healing agent was sprayed at the lamina interface so that a small amount of vitrimer healing agent can repeatedly heal delamination induced by low velocity impact. Because the matrix was a SMP with flame retardancy, the composite laminate exhibited multifunctionalities. The vitrimer powder particles endowed the laminate with improved resistance to crack initiation and propagation, enhanced interlamina strength, and repeated self-healing capability. The composite laminates exhibited significant delamination healing/recycling efficiencies, with first cycle efficiency of 98.0% and second cycle healing efficiency of 85.9% in terms of critical buckling loads. The GFRP-TAITPOVP laminate also had a high recovery stress of 65.6 MPa. In addition, the 7 wt% TPO gave rise to an efficient flame retardancy to the composite laminate, which validates the synergy between the phosphine oxide structures, and the isocyanurate ring. The high

thermal stability, excellent mechanical properties, and multifunctionalities suggested that the laminate can be used in harsh environments. We believe that this multifunctional composite laminate can be used sustainably in many engineering applications such as lightweight aerospace structures, deployable structures, and structures with fire hazard.

Data availability statement

All data that support the findings of this study are included within the article (and any supplementary files).

Acknowledgments

This work is supported by the US National Science Foundation under Grant Number OIA-1946231 and the Louisiana Board of Regents for the Louisiana Materials Design Alliance (LAMDA), and the National Science Foundation under Grant Number HRD-1736136.

Conflict of interest

The authors declare no conflict of interest

Author contributions

J K contributed towards the specimen preparation, data generation, testing and characterization, data analysis, and draft manuscript preparation. X F designed and prepared the vitrimer healing agent and revised the manuscript. G L initiated the concept, raised funding for the work, guided the research, and co-wrote the manuscript.

ORCID iD

Guoqiang Li https://orcid.org/0000-0002-7004-6659

References

[1] Tian Y, Wang Q, Hu Y, Sun H, Cui Z, Kou L, Cheng J and Zhang J 2019 Preparation and shape memory properties of rigid-flexible integrated epoxy resins via tunable micro-phase separation structures *Polymer* **178** 121592
[2] Luo J, Yang S, Lei L, Zhao J and Tong Z 2017 Toughening, synergistic fire retardation and water resistance of polydimethylsiloxane grafted graphene oxide to epoxy nanocomposites with trace phosphorus *Composites* A **100** 275–84
[3] Malekzadeh Fard K, Khalili S M R, Forooghy S H and Hosseini M 2014 Low velocity transverse impact response of a composite sandwich plate subjected to a rigid blunted cylindrical impactor *Composites* B **63** 111–22
[4] Zainuddin S, Arefin T, Fahim A, Hosur M V, Tyson J D, Kumar A, Trovillion J and Jeelani S 2014 Recovery and improvement in low-velocity impact properties of e-glass/epoxy composites through novel self-healing technique *Compos. Struct.* **108** 277–86
[5] Prasath K A, Arumugaprabu V, Amuthakkannan P, Manikandan V and Deepak Joel Johnson R 2020 Low velocity impact, compression after impact and morphological studies on flax fiber reinforced with basalt powder filled composites *Mater. Res. Express* **7** 015317
[6] Dai X, Du Y, Wang Y, Liu Y, Xu N, Li Y, Shan D, Xu B D, Xu B B and Kong J 2020 Stretchable self-healing polymeric networks with recyclability and dual responsiveness *ACS Appl. Polym. Mater.* **2** 1065–72
[7] Zhang H, Cui J, Hu G and Zhang B 2022 Recycling strategies for vitrimers *Int. J. Smart Nano Mater.* **13** 367–90
[8] Wang X, Lu H, Liu X, Hossain M, Fu Y Q and Xu B B 2020 Dynamic coordination of miscible polymer blends towards highly designable shape memory effect *Polymer* **208** 122946
[9] Li G 2014 *Self-Healing Composites: Shape Memory Polymer Based Structures* (West Sussex: John Wiley & Sons, Inc)
[10] Yao Y, Wang J, Lu H, Xu B, Fu Y, Liu Y and Leng J 2016 Thermosetting epoxy resin/thermoplastic system with combined shape memory and self-healing properties *Smart Mater. Struct.* **25** 015021
[11] White S R, Sottos N R, Geubelle P H, Moore J S, Kessler M R, Sriram S R, Brown E N and Viswanathan S 2001 Autonomic healing of polymer composites *Nature* **409** 794–7
[12] Lee J, Zhang M, Bhattacharyyaa D, Yuan Y, Jayaramana K and Mai Y 2012 Micromechanical behavior of self-healing epoxy and hardener-loaded microcapsules by nanoindentation *Mater. Lett.* **76** 62–65
[13] Pang J W C and Bond I P 2005 A hollow fibre reinforced polymer composite encompassing self-healing and enhanced damage visibility *Compos. Sci. Technol.* **65** 1791–9
[14] Trask R S, Williams G J and Bond I P 2007 Bioinspired self-healing of advanced composite structures using hollow glass fibres *J. R. Soc. Interfaces* **4** 363–71
[15] Toohey K S, Sottos N R, Lewis J A, Moore J S and White S R 2007 Self-healing materials with microvascular networks *Nat. Mater.* **6** 581–5
[16] Williams H R, Trask R S, Knights A C, Williams E R and Bond I P 2008 Biomimetic reliability strategies for self-healing vascular networks in engineering materials *J. R. Soc. Interfaces* **5** 735–47
[17] Hayes S A, Jones F R, Marshiya K and Zhang W 2007 A self-healing thermosetting composite material *Composites* A **38** 1116–20
[18] Hayes S A, Zhang W, Branthwaite M and Jones F R 2007 Self-healing of damage in fibre-reinforced polymer-matrix composites *J. R. Soc. Interfaces* **4** 381–7
[19] Nji J and Li G 2010 A biomimic shape memory polymer based self-healing particulate composite *Polymer* **51** 6021–9
[20] John M and Li G 2010 Self-healing of sandwich structures with grid stiffened shape memory polymer syntactic foam core *Smart Mater. Struct.* **19** 075013
[21] White S R, Moore J S, Sottos N R, Krull B P, Santa Cruz W A and Gergely R C R 2014 Restoration of large damage volumes in polymers *Science* **344** 620–3
[22] Nji J and Li G 2012 Damage healing ability of a shape memory polymer based particulate composite with small thermoplastic contents *Smart Mater. Struct.* **21** 025011
[23] Li G and Nettles D 2010 Thermomechanical characterization of a shape memory polymer based self-repairing syntactic foam *Polymer* **51** 755–62
[24] Li G and Uppu N 2010 Shape memory polymer based self-healing syntactic foam: 3-D confined thermomechanical characterization *Compos. Sci. Technol.* **70** 1419–27
[25] Montarnal D, Capelot M, Tournilhac F and Leibler L 2011 Silica-like malleable materials from permanent organic networks *Science* **334** 965–8

[26] Liu T, Zhao B and Zhang J 2020 Recent development of repairable, malleable and recyclable thermosetting polymers through dynamic transesterification *Polymer* **194** 122392

[27] Denissen W, Winne J W and Prez F E D 2016 Vitrimers: permanent organic networks with glasslike fluidity *Chem. Sci.* **7** 30–38

[28] Guerre M, Taplan C, Winne J W and Prez F E D 2020 Vitrimers: directing chemical reactivity to control material properties *Chem. Sci.* **11** 4855–70

[29] Lu L, Fan J and Li G 2016 Intrinsic healable and recyclable thermoset epoxy based on shape memory effect and transesterification reaction *Polymer* **105** 10–18

[30] Lu L, Pan J and Li G 2017 Recyclable high performance epoxy based on transesterification reaction *J. Mater. Chem.* A **5** 21505–13

[31] Li A, Fan J and Li G 2018 Recyclable thermoset shape memory polymer with high stress and energy output via facile UV-curing *J. Mater. Chem.* A **6** 11479–87

[32] Li A, Challapalli A and Li G 2019 4D printing of recyclable lightweight architectures using high recovery stress shape memory polymer *Sci. Rep.* **9** 7621

[33] Yue L, Guo H, Kennedy A, Patel A, Gong X, Ju T, Gray T and Manas-Zloczower I 2020 Vitrimerization: converting thermoset polymers into vitrimers *ACS Macro Lett.* **9** 836–42

[34] Ma J, Porath L E, Haque M, Sett S, Rabbi K F, Nam S, Miljkovic N and Evans C M 2021 Ultra-thin self-healing vitrimer coatings for durable hydrophobicity *Nat. Commun.* **12** 5210

[35] Röttger M, Domenech T, van Der Weegen R, Breuillac A, NicolaŸ R and Leibler L 2017 High-performance vitrimers from commodity thermoplastics through dioxaborolane metathesis *Science* **356** 62–65

[36] van Zee N and Nicolaÿ R 2020 Vitrimers: permanently crosslinked polymers with dynamic network topology *Prog. Polym. Sci.* **104** 101233

[37] Feng X and Li G 2020 Versatile phosphate diester based flame retardant vitrimers via catalyst-free mixed transesterification *ACS Appl. Mater. Interfaces* **12** 57486–96

[38] Feng X and Li G 2021 Catalyst-free β-hydroxy phosphate ester exchange for robust fire-proof vitrimers *Chem. Eng. J.* **417** 129132

[39] Feng X and Li G 2021 Room-temperature self-healable and mechanically robust thermoset polymer for healing delamination and recycling carbon fiber *ACS Appl. Mater. Interfaces* **13** 53099–110

[40] Feng X, Fan J, Li A and Li G 2020 Biobased tannic acid crosslinked epoxy thermosets with hierarchical molecular structure and tunable properties: damping, shape memory and recyclability *ACS Sustain. Chem. Eng.* **8** 874–83

[41] Feng X, Fan J, Li A and Li G 2019 Multi-reusable thermoset with anomalous flame triggered shape memory effect *ACS Appl. Mater. Interfaces* **11** 16075–86

[42] Feng X and Li G 2021 High-temperature shape memory photopolymer with intrinsic flame retardancy and record-high recovery stress *Appl. Mater. Today* **23** 101056

[43] Santo L, Taleghani A D and Li G 2018 Expandable proppants to moderate production drop in hydraulically fractured wells *J. Nat. Gas Sci. Eng.* **55** 182–90

[44] Elhag M, Salehi S, Li G, Fan J and Teodoriu C 2021 Loss circulation prevention in geothermal drilling by shape memory polymer *Geothermics* **89** 101943

[45] Li G and Xu T 2011 Thermomechanical characterization of shape memory polymer based self-healing syntactic foam sealant for expansion joint *ASCE J. Transp. Eng.* **137** 805–14

[46] Delaey J, Dubruel P and van Vlierberghe S 2020 Shape-memory polymers for biomedical applications *Adv. Funct. Mater.* **30** 1909047

[47] Basak S 2021 Redesigning the modern applied medical sciences and engineering with shape memory polymers *Adv. Compos. Hybrid Mater.* **4** 1–12

[48] Yang H, Shi R, Jiang Q and Ren J 2023 Properties and mechanism of two-way shape memory polyurethane composite under stress-free condition *Adv. Compos. Hybrid Mater.* **6** 1

[49] Gao H, Li J, Liu Y and Leng J 2021 Shape memory polymer solar cells with active deformation *Adv. Compos. Hybrid Mater.* **4** 957–65

[50] Zhang H *et al* 2022 Multi-functional phase change materials with anti-liquid leakage, shape memory, switchable optical transparency and thermal energy storage *Adv. Compos. Hybrid Mater.* **5** 2042–50

[51] Lan X, Liu Y, Lv H, Wang X, Leng J and Du S 2009 Fiber reinforced shape-memory polymer composite and its application in a deployable hinge *Smart Mater. Struct.* **18** 024002

[52] Afful H Q, Ibekwe S, Mensah P and Li G 2021 Influence of uniaxial compression on the shape memory behavior of vitrimer composite embedded with tension-programmed unidirectional shape memory polymer fibers *J. Appl. Polym. Sci.* **138** 50429

[53] Konlan J, Mensah P, Ibekwe S, Crosby K and Li G 2020 Vitrimer based composite laminates with shape memory alloy Z-pins for repeated healing of impact induced delamination *Composites* B **200** 108324

[54] Taplan C, Guerre M and Du Prez E 2021 Covalent adaptable networks using β-amino esters as thermally reversible building blocks *J. Am. Chem. Soc.* **143** 9140–50

[55] Sáenz-Pérez M, Laza J M, García-Barrasa J, Vilas J L and León L M 2018 Influence of the soft segment nature on the thermomechanical behavior of shape memory polyurethanes *Polym. Eng. Sci.* **58** 238–44

[56] Behl M, Razzaq M Y and Lendlein A 2013 Tailoring the recovery force in magnetic shape-memory nanocomposites *Mater. Res. Soc. Symp.* **1569** 129–34

[57] Lu H, Yu K, Liu Y and Leng J 2010 Sensing and actuating capabilities of a shape memory polymer composite integrated with hybrid filler *Smart Mater. Struct.* **19** 065014

[58] Ji F L, Hu J L, Yu W M W and Chiu S S Y 2011 Structure and shape memory properties of polyurethane copolymers having urethane chains as soft segments *J. Macromol. Sci.* B **50** 2290–306

[59] Lu H, Wang X, Yao Y, Gou J, Hui D, Xu B and Fu Y Q 2015 Synergistic effect of siloxane modified aluminum nanopowders and carbon fiber on electrothermal efficiency of polymeric shape memory nanocomposite *Composites* B **80** 1–6

[60] Xu B, Fu Y Q, Huang W M, Pei Y T, Chen Z G, De Hosson J T M, Kraft A and Reuben R L 2010 Thermal-mechanical properties of polyurethane-clay shape memory polymer nanocomposites *Polymers* **2** 31–39

[61] Fan J and Li G 2018 High enthalpy storage thermoset network with giant stress and energy output in rubbery state *Nat. Commun.* **9** 642

[62] Xia Y, He Y, Zhang F, Liu Y and Leng J 2021 A review of shape memory polymers and composites: mechanisms, materials, and applications *Adv. Mater.* **33** 2000713

[63] Agarwal B D, Broutman L J and Chandrashekhara K 2006 *Analysis and Performance of Fiber Composites* 3rd edn (Hoboken, NJ: Wiley)

[64] Konlan J, Mensah P, Ibekwe S and Li G 2022 A laminated vitrimer composite with strain sensing, delamination self-healing, deicing, and room-temperature shape restoration properties *J. Compos. Mater.* **56** 2267–78

[65] Liu K and Macosko C W 2019 Can nanoparticle toughen fiber-reinforced thermosetting polymers? *J. Mater. Sci.* **54** 4471–83

[66] Nayak S, Nayak R K and Panigrahi I 2022 Effect of nano-fillers on low-velocity impact properties of synthetic and natural fibre reinforced polymer composites- a review *Adv. Mater. Process. Technol.* **8** 2963–86

[67] Landowski M, Strugała G, Budzik M and Imielińska K 2017 Impact damage in SiO_2 nanoparticle enhanced epoxy—carbon fibre composites *Composites* B **113** 91–99

[68] Li G and Chakka V S 2010 Isogrid stiffened syntactic foam cored sandwich structure under low velocity impact. *Composites* A **41** 177–84

[69] Feng X, Wang X, Cai W, Qiu S, Hu Y and Liew K M 2016 Studies on synthesis of electrochemically exfoliated functionalized graphene and polylactic acid/ferric phytate functionalized graphene nanocomposites as new fire hazard suppression materials *ACS Appl. Mater. Interfaces* **8** 25552–62

[70] Khanal S, Zhang W, Ahmed S, Ali M and Xu S 2018 Effects of intumescent flame retardant system consisting of tris (2-hydroxyethyl) isocyanurate and ammonium polyphosphate on the flame retardant properties of high-density polyethylene composites. *Composites* A **112** 444–51